1 Fabrication

Our device fabrication process begins with ultra-high resistivity Si wafers: $\langle 100 \rangle$ orientation, 500 micrometers thick. The wafer is coated with 70nm of silicon nitride (high stress, low pressure chemical vapor deposited) which will form the nanoresonator substrate material. As we have found this material to have high microwave dissipation, the SiN is etched away from all but small $2\mu m$ x $37\mu m$ islands where the nanoresonators will be fabricated. This is accomplished using photolithographic patterning and a combination of CHF_3/O_2 plasma etching and a 6:1 buffered oxide wet etch.

The resulting SiN islands are then coated with 80nm of aluminum, using photolithography and lift-off. The Al serve a dual purpose as a stop-etch barrier and as pads for electrical contact with the subsequent niobium deposition. 350nm of niobium is deposited over the entire wafer in a low pressure($2 \cdot 10^{-7}$ torr) sputter system. The niobium is then etched to form the coplanar wave guide and resonator using a CF_4/O_2 plasma with a photoresist etch mask. This process etches slightly into the silicon over most of the device but is stopped by the aluminum stop-etch at the SiN islands.

Following the niobium etch, the aluminum is patterned to leave small electrical contact pads, using photolithography followed by wet etching with an aluminum stripping solution. The nanoresonators are then formed in a two step e-beam process. First, using a bilayer PMMA mask, e-beam lithography, aluminum evaporation, followed by liftoff, the nanoresonator, gate, and electrical contacts to the niobium are defined. A second e-beam process then defines an etch window in a PMMA mask located around the nanoresonator. The mechanical resonator is freed via a two-step etch process. The first etch, CHF_3/O_2, vertically removes the SiN layer, and the the second, an SF_6 etch, isotropically under-etches and frees the beam. The finished chips are cleaned in O_2 plasma before mounting in sample boxes.

2 Calibration and cavity photon measurement

From a circuit model [1], [2], we can directly derive the power in sidebands generated through nanomechanical motion modulating the SR capacitance.

$$P_m = P_{in} \cdot \frac{4\kappa_R\kappa_L}{\kappa^2 + 4(\omega_p - \omega_{SR})^2} \left(\frac{1}{2C}\frac{dC_g}{dx}Q\right)^2 \cdot 2\left\langle x^2\right\rangle \cdot \quad (1)$$

$$= P_{in} \cdot \frac{4\kappa_R\kappa_L}{\kappa^2 + 4(\omega_p - \omega_{SR})^2} \left(\frac{d\omega_{SR}}{dx}\frac{1}{\kappa}\right)^2 \cdot 2\left\langle x^2\right\rangle \cdot \quad (2)$$

$$= P_{out} \cdot \left(\frac{d\omega_{SR}}{dx}\frac{1}{\kappa}\right)^2 \cdot 2\left\langle x^2\right\rangle \cdot \quad (3)$$

Where P_{in} is power incident on the input of the cavity, P_{out} is power directly at the output of the cavity, κ is total cavity linewidth, and $\kappa_{ext} = \kappa_R + \kappa_L$ is linewidth due to the external loading of the cavity by the two end coupling capacitors. It is generally assumed that $\kappa_L = \kappa_R$.

Using a weak probe signal and assuming the nanoresonator motion follows equipartition, $\frac{1}{2}k\left\langle x^2\right\rangle = \frac{1}{2}k_BT$, we can obtain a calibration of the sideband signal to mechanical motion and temperature, as shown in fig 1b in the paper. Using this calibration referenced to output power, which we directly measure, along with an estimate of the nanoresonator effective spring constant, we can extract the coupling constant. To determine spring constant, we first make a best estimate of the nanoresonator effective mass based upon known layer thicknesses and careful SEM measurements of beam and gate dimensions, as well as a geometric mass conversion factor which in our case is approximately unity[3], and then use the relation $\omega_m^2 = \frac{k}{m_{eff}}$. This gives $m_{eff} \approx 2pg$, $k \approx 3.2N/m$, and a coupling of $\frac{d\omega_{SR}}{dx} \approx 84\mathrm{K}Hz/nm$. This technique has the advantage of being directly proportional to the ratio of P_m/P_{out} which we measure to high accuracy, rather than relying on any additional knowledge of line losses or gains.

To extract the number of microwave pump photons in the cavity we use the relation:

$$\bar{n}_p = P_{in}\frac{4\kappa_R\kappa_L}{\kappa^2 + 4(\omega_p - \omega_{SR})^2}\frac{1}{\kappa_R}\frac{1}{\hbar\omega_p} \tag{4}$$

$$= P_{out}\cdot\frac{1}{\kappa_R}\cdot\frac{1}{\hbar\omega_p} \tag{5}$$

where it is assumed that $\kappa_L = \kappa_R$. Through careful measurements of total loss/gain in our measurement system from the output of the cavity to the spectrum analyzer, as well as by calibrating background noise levels with known noise temperature of the HEMT amplifier, we can determine P_{out}. Ideally, if the superconducting resonator is dominated by external loading, $\kappa_{ext} = \kappa$ can be directly measured through swept transmission measurements of the cavity[3]. However, this sample had some degree of additional internal loss, which required a careful measurement of κ_{ext}.

To determine κ_{ext} we use the nanoresonator as a calibrated energy source. Given a coupling to the cavity of $\Gamma_{opt} = \Gamma_{tot} - \Gamma_m^T$, the total power that escapes out the output port of the cavity is given by:

$$P_{sideb} = \hbar\omega_{SR}\bar{n}_m\Gamma_{opt}\left(\frac{\kappa_R}{2\kappa}\right) \tag{6}$$

Using this to extract κ_R and comparing over a broad range of nanoresonator mode temperatures and Γ_{opt} gives consistent results. With this, we can then directly relate $\bar{n}_p$ to measured output power using eq. 5.

In a similar fashion, we can measure $\bar{n}_{SR}$. Rather than measuring a single coherent signal, however, we must measure the total power output from the cavity. We do this by taking a wide spectrum measurement on a spectrum analyzer and fitting the resultant Lorentzian lineshape to extract total power. An example of this type of measurement is seen in Fig 1. This measured power is then directly referred to $\bar{n}_{SR}$ in the same fashion as eq. 5.

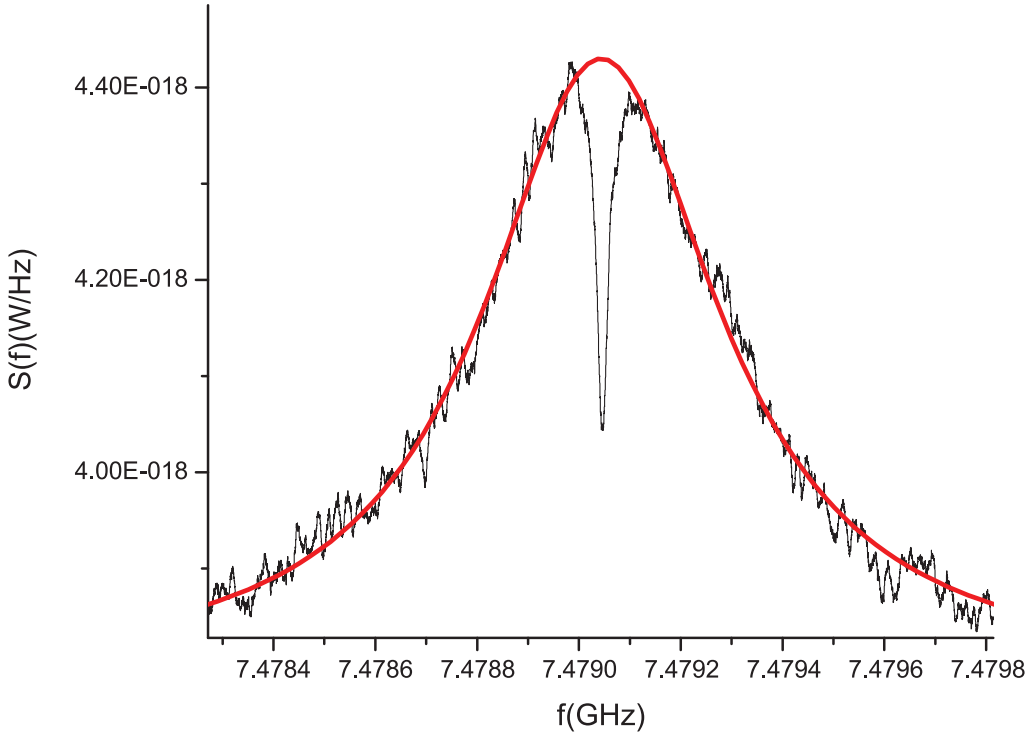

Figure 1: Wide spectrum measurement of cavity photon occupation. $n_p \approx 3 \cdot 10^9$, $\bar{n}_{SR} \approx 3$. The nanoresonator sideband can be clearly seen and is masked out when fitting the cavity Lorentzian.

3 Calibration linearity and stability

To address any concerns that the equipartition-derived position calibration is either non-constant over time or non-linear with applied pump power we have done several additional measurements. First, measurement of thermal motion taken over hours or days consistently follow the equipartition relation found in the thermal calibration. Even warming the sample to 77K and back to 150mK gives consistent behavior before and after warmup. In addition, we have measured the response of the nanoresonator continuously over 10 hours and found a constant response with $< 2\%$ scatter.

To measure linearity of the calibration with applied pump power, we have done two things. First, we directly measure the power transmitted through the cavity at the pump frequency and have found this to be directly linear with applied power to within the uncertainties of our measurement. This directly implies that neither cavity κ nor frequency are changing with power to within $\sim 5\%$. In addition, we directly measure the transmission response of the cavity using a network analyzer while adding in the red pump. From this, we determine that cavity frequency is unchanging, while κ changes by $\sim \pm 2.5\%$.

As a more definitive test, we can directly drive the nanoresonator with a known force noise and observe that the response agrees with expectations. Using the equipartition theorem and the nanoresonator's Lorentzian response to a force, we can directly derive an effective temperature T_{eff} that a purely random force noise spectrum would drive the nanoresonator to:

$$T_{eff} = \frac{\omega_m^2}{4k_B k \Gamma_{tot}} S_F \tag{7}$$

where Γ_m^{tot} is the total(observed) linewidth of the nanoresonator and S_F is then applied force noise in N^2/Hz.

We can generate this force noise by directly applying a voltage noise to the cavity. Given a voltage, V, on the superconducting resonator, the force on the nanoresonator is given by $F = -\frac{\partial E}{\partial x} = \frac{1}{2} V^2 \frac{\partial C}{\partial x}$. We drive with a known force noise by applying random voltage noise at 1MHz combined with a pure tone at 5MHz, which combine to produce a random force noise at the nanoresonator frequency. This avoids any complications of the $\sim$1mV DC

offset voltage typically observed in our device. We generate these signals using the filtered output of a high sample rate arbitrary function generator with a sufficiently long noise repetition rate to produce effective white noise. The measured effective temperature and magnitude of the nanoresonator motion produced in this fashion agrees with our estimates of line loss and device parameters.

Driving with a constant applied force noise spectral density, we can measure T_{eff} vs applied red pump strength. The resultant data can be seen in the paper, Fig. 2. Taking this data and multiplying by the measured Γ_{tot} for each point should give us a constant from which any deviations can be attributed to changes in our position calibration. Doing this, we find deviations of less than $\pm 3.5\%$ over our entire power range. We factor this uncertainty into our error analysis of nanoresonator temperature.

4 Pump detuning measurements

Sweeping the red pump frequency from exactly $\omega_{SR} - \omega_m$ and observing the frequency shift of the nanomechanics, the so-called optical spring effect, gives an additional method of verifying device behavior as well as the coupling strength.

From [4] we obtain the optomechanical frequency pulling. In addition, we find that the frequency pulling must include a term directly proportional to applied power. This can be attributed to an electrostatic type frequency pulling proportional to the average square of the voltage of the microwave field in the cavity. The entire frequency shift due to applied power is then given by:

$$\Delta\omega_{tot}^{NR} = \left(-\lambda x_{zp}^2 + \frac{2(g^2 x_{zp}^2 \delta \left[\left(\frac{\kappa}{2}\right)^2 + \delta^2 - \omega_m^2 \right]}{\left[\left(\frac{\kappa}{2}\right)^2 + (\omega_m + \delta)^2 \right] \left[\left(\frac{\kappa}{2}\right)^2 + (\omega_m - \delta)^2 \right]} \right) \bar{n}_p \qquad (8)$$

Where g is coupling constant, $x_{zp} = \sqrt{\hbar/2m\omega_m}$ is zero point motion, $\delta = \omega_p - \omega_m$ is pump detuning, and $\lambda = \frac{1}{2}\frac{\omega_{SR}}{C_{tot}}\frac{\partial^2 C_g}{\partial x^2}$ is the second order frequency

pulling term. Fitting detuning data of this type(Fig. 2) gives a coupling in agreement with that found from our thermal calibration and $\lambda = 2\pi \cdot 1.2 \pm 0.7\text{KHz/nm}^2$.

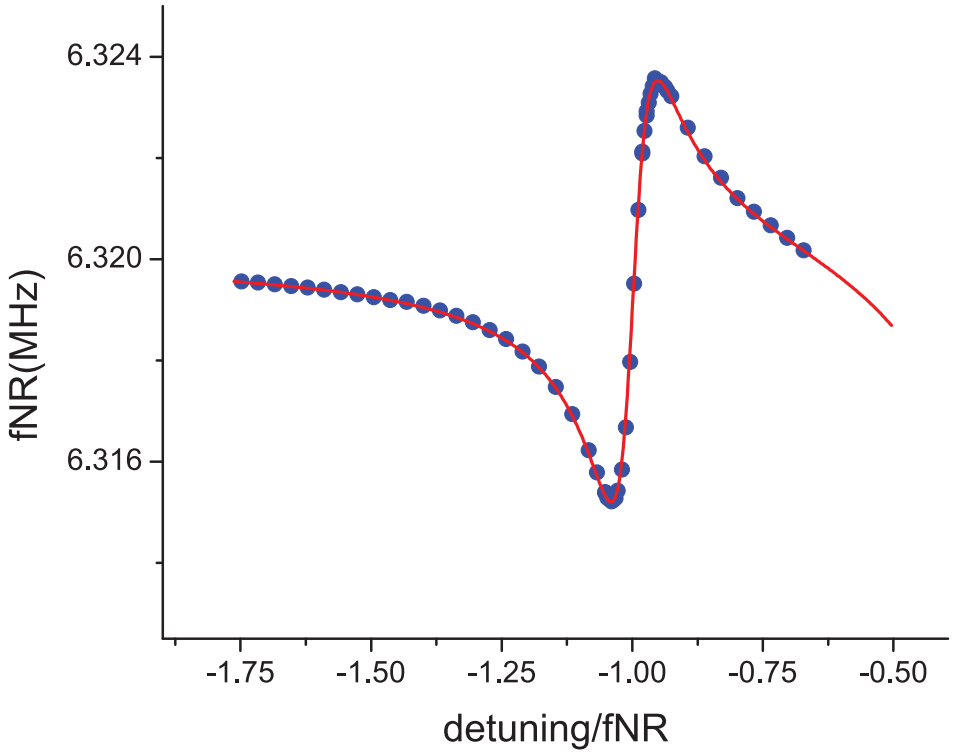

Figure 2: Detuning data. Applied power is held constant while frequency is swept, producing a changing $\bar{n}_p$

5 Comparison with previous work

The experiment we present is similar to that of Teufel et al[5] which demonstrated cooling from $\bar{n}_m = 700$ to 200. To better illustrate differences and improvements in our presented work, we can a make a brief comparison of the

experiments and devices. The largest fundamental difference is that our microwave resonator is designed with double end-coupling capacitors allowing direct measurement in transmission mode, rather than the interferometer-type measurements of Teufel et al. Our design provides several favorable features, in particular the reduction of red-detuned drive power transmitted to the amplifier, reducing the complication of amplifier saturation. In addition, our microwave resonators are constructed of niobium rather than aluminum for higher power handling.

The significantly improved cooling demonstrated here is primarily produced through greatly increased NR-SR coupling and power handling. For a numerical comparison, the experiment of Teufel et al demonstrated a coupling of $6.4KHz/nm$, NR frequency of $1.525MHz$, and a maximum demonstrated circulating power of $7.3uW$. By comparison, we have demonstrated a coupling of $\sim 80KHz/nm$, NR frequency of $6.2MHz$, and a maximum photon count of $2 \cdot 10^9$ photons, equivalent to $468uW$ circulating power.

6 Theoretical results

The basic backaction cooling mechansim we use here was first described in Ref. [6]; a fully quantum theory demonstrating that one could cool to the ground state was presented in Refs. [7, 8], with further details presented in Refs. [9, 10]. This general approach can easily be extended to describe the situation relevant to our experiments, where one must include the effects of thermal excitation of the superconducting cavity (SR). The effects of thermal cavity excitation on the minimal possible temperature achievable via backaction cooling was previously studied in Ref. [10]. Unlike that work, we will also be interested in understanding the form of the cavity output spectrum when there is thermal noise in the cavity.

We consider a two-sided high-Q cavity coupled to a high-Q mechanical resonator via the Hamiltonian given in Eq. 1 of the main text. We will ignore the effects of the electrostatic frequency-pulling term $\propto \lambda$ in this Hamiltonian, as for the chosen drive configuration, this term is far off-resonance. The cavity damping rate κ may be decomposed as $\kappa = \kappa_L + \kappa_R + \kappa_I$, where κ_L, κ_R correspond to the coupling to the input (L) and output (R) ports of the cavity, and κ_I corresponds to additional dissipative channels coupled to the cavity (i.e. internal losses). The dissipative ports are treated in the standard way using input-output theory [11]. Further, we linearize the cavity field about its classical amplitude $\bar{a}$ in the usual way, $\hat{a}(t) = e^{-i\omega_p t}\left(\bar{a} + \hat{d}(t)\right)$. The effective optomechanical coupling constant α is defined as:

$$\alpha = \frac{d\omega_{sr}}{dx} x_{zp} \bar{a}, \tag{9}$$

while $\Delta = \omega_p - \omega_{sr}$ describes the detuning of the pump. We introduce the bare mechanical susceptibility $\chi_m(\omega) = (-i(\omega - \omega_m) + \Gamma_m^T/2)^{-1}$ and cavity susceptibility $\chi_{sr}(\omega) = (-i(\omega + \Delta) + \kappa/2)^{-1}$. Further defining $\bar{\chi}_m(\omega) = \chi_m^*(-\omega)$, $\bar{\chi}_{sr}(\omega) = \chi_{sr}^*(-\omega)$, the solution of the linearized Heisenberg equations of motion for the mechanical oscillator annihilation operator $\hat{c}$ takes the form:

$$\hat{c}[\omega] = \tilde{\chi}_m[\omega]\left(-\sqrt{\Gamma_m^T}\hat{\eta}[\omega] - i\alpha \sum_{j=L,R,I} \sqrt{\kappa_j}\left(\chi_{sr}[\omega]\hat{\xi}_j[\omega] + \bar{\chi}_{sr}[\omega]\hat{\xi}_j^\dagger[\omega]\right)\right) \tag{10}$$

$$\tilde{\chi}_m(\omega) = \frac{\chi_m(\omega)}{1 + i\chi_m(\omega)\Sigma(\omega)} \tag{11}$$

Here, $\tilde{\chi}_m[\omega]$ represents the mechanical susceptibility in the presence of the cavity backaction, and is defined in terms of the self-energy:

$$\Sigma(\omega) = -i|\alpha|^2\left(\chi_{sr}(\omega) - \bar{\chi}_{sr}(\omega)\right) \tag{12}$$

$\hat{\eta}$ is the noise associated with the intrinsic mechanical damping, and satisfies:

$$\langle \hat{\eta}^\dagger(t)\hat{\eta}(0)\rangle = \bar{n}_m^T \delta(t) \tag{13}$$

$$\langle \hat{\eta}(t)\hat{\eta}^\dagger(0)\rangle = \left(1 + \bar{n}_m^T\right)\delta(t) \tag{14}$$

where $\bar{n}_m^T$ represents the temperature of the intrinsic dissipative bath coupled to the mechanical resonator (expressed as a number of quanta). If there were no coupling to the cavity, the mechanical resonator would be in a thermal state with an average number of qunta $\bar{n}_m^T$.

In a similar fashion, $\hat{\xi}_L, \hat{\xi}_R$ and $\hat{\xi}_I$ describes the noise entering the cavity from the three dissipative channels coupled to the resonator ($j = L, R, I$):

$$\langle \hat{\xi}_j^\dagger(t)\hat{\xi}_j(0)\rangle = \bar{n}_j^T \delta(t) \quad (15)$$

$$\langle \hat{\xi}_j(t)\hat{\xi}_j^\dagger(0)\rangle = \left(1+\bar{n}_j^T\right)\delta(t) \quad (16)$$

Here, $\bar{n}_j^T$ represents the temperature of the dissipative bath j, expressed as always as a number of mechanical oscillator quanta. In the ideal case, one has $\bar{n}_L^T = \bar{n}_R^T = \bar{n}_I^T = 0$, implying that the only noise driving the cavity is vacuum noise. In the presence of thermal noise, the cavity will have a non-zero number of thermal quanta, given by:

$$\bar{n}_{sr}^T = \frac{1}{\kappa}\sum_{j=L,R,I}\kappa_j \bar{n}_j^T \quad (17)$$

Note that the self energy $\Sigma[\omega]$ is not affected by the presence of thermal noise driving the cavity, and has the same form given as Ref. [7]; as such, the optomechanical damping and frequency shift have no dependence on the thermal noise driving the cavity. Note also that the high-Q of both the cavity and mechanical resonator allow us to safely treat the various noises driving the cavity as being effectively white.

6.1 Mechanical resonator occupancy

We can now find the temperature of the oscillator (expressed as a number of quanta $\bar{n}_m$) via equipartition:

$$1 + 2\bar{n}_m \equiv \frac{\langle \hat{x}^2\rangle}{x_{zp}^2} = \frac{1}{x_{zp}^2}\int_{-\infty}^{\infty}\frac{d\omega}{2\pi}S_{xx}[\omega] = \frac{1}{x_{zp}^2}\int_{-\infty}^{\infty}\frac{d\omega}{2\pi}\frac{\langle \hat{x}[\omega]\hat{x}[\omega']\rangle}{2\pi\delta(\omega-\omega')} \quad (18)$$

Using the solution for $\hat{c}[\omega]$, and assuming an optimal detuning for cooling, $\Delta = -\omega_m$, we have:

$$\bar{n}_m = \frac{\Gamma_m^T}{\Gamma_m^T + \Gamma_{\rm opt}}\bar{n}_m^T + \frac{\Gamma_{\rm opt}}{\Gamma_m^T + \Gamma_{\rm opt}}\bar{n}_{sr}^{BA}. \quad (19)$$

Here, the optical damping of the mechanics is given by:

$$\Gamma_{\rm opt} = \frac{4|\alpha|^2}{\kappa}\frac{1}{1+(\kappa/(4\omega_m))^2} \quad (20)$$

while the effective number of quanta associated with the cavity backaction is given in the relevant limit $\Gamma_{\rm opt} \ll \kappa$ by:

$$\bar{n}_{sr}^{BA} = \left(\frac{\kappa}{4\omega_m}\right)^2 + \bar{n}_{sr}^{T}\left[1+2\left(\frac{\kappa}{4\omega_m}\right)^2\right]. \quad (21)$$

As noted in Ref. [10], the effective backaction occupancy $\bar{n}_{sr}^{BA}$ cannot be any lower than the thermal occupancy of the cavity, $\bar{n}_{sr}^{T}$.

6.2 Output spectrum

We now turn to a calculation of the output spectrum of the microwaves leaving the cavity through the right port. We assume the situation relevant to the experiment, where the coherent drive is applied to the cavity from the left port. Further, we assume that no extraneous thermal noise enters the cavity from the output R port, but only from the drive (L) port and the from dissipative bath responsible for the cavity's internal losses (the I port). As discussed in the main text, we expect that the excess thermal noise driving the cavity is almost entirely associated with its internal losses, i.e. κ_I. Further, as there are no large powers associated with the output (right) port, it is extremely unlikely that thermal noise enters the cavity via this coupling. We thus take $\bar{n}_R^T = 0$ in what follows, implying $\bar{n}_{sr}^T = (\kappa_I/\kappa)\bar{n}_I^T + (\kappa_L/\kappa)\bar{n}_L^T$.

Standard input/output theory [12] gives us the following expression for the output field leaving the cavity via the waveguide coupled to its output port:

$$\hat{b}_{{\rm out},R}(t) = \hat{\xi}_R(t) + \sqrt{\kappa_R}\hat{a}(t) \quad (22)$$

where $\hat{a}$ is the cavity annihilation operator. Note that the output field is defined so that the average power associated with the output is given by:

$$P_{\rm out}(t) = \hbar\omega_p\langle\hat{b}_{{\rm out},R}^{\dagger}(t)\hat{b}_{{\rm out},R}(t)\rangle \quad (23)$$

(see Appendix D of [12]).

Without loss of generality, we chose the phase of the cavity drive to make $\bar{a} \equiv \langle \hat{a} \rangle$ real. Using the solution to the linearized Heisenberg equations of motion for $\hat{c}[\omega]$ and $\hat{d}[\omega]$, we find that the noise in the output field is given by:

$$\begin{aligned}\left(\hat{b}_{\mathrm{out},R}[\omega]\right)_{\mathrm{noise}} &= \hat{\xi}_R[\omega] - \\ &\sqrt{\kappa_R}\chi_{sr}[\omega]\sum_j \sqrt{\kappa_j}\left(1-\alpha^2\tilde{\chi}_m[\omega]\chi_{sr}[\omega]\right)\hat{\xi}_j \\ &-\sqrt{\kappa_R\Gamma_m^T}\chi_{sr}[\omega](i\alpha)\tilde{\chi}_m[\omega]\hat{\eta} \end{aligned} \quad (24)$$

We have simplified the above expression by taking the relevant limit where the the total mechanical damping is much smaller than ω_m; this is equivalent to making a rotating wave-approximation in the cavity-mechanics interaction. Each term in the above equation for the output field has a simple meaning. The first term tells us that if there was no coupling to the cavity ($\kappa_R \to 0$), the noise incident on the cavity from the right would just be reflected back. The terms on the second line correspond to the cavity responding to the noise entering from both drive ports ($j = L, R$) as well as from the dissipative bath reponsible for the internal cavity loss ($j = \mathrm{int}$). In particular, note the prefactor of $\hat{\xi}_j$. The two terms in the brackets correspond (respectively) to the direct influence of the drive noise on the cavity, and the back-action effect of this noise (i.e. the noise $\hat{\xi}_j$ first drives the cavity, which in turn drives the mechanics, which in turn drives the cavity). Finally, the last line corresponds to equilibrium noise driving the mechanics, which then drives the cavity, and then contributes to the output noise.

We can now calculate the power spectrum associated with the output field leaving the cavity from the right. We first consider the standard output power spectrum defined as:

$$S_R[\omega] \equiv \int_{-\infty}^{\infty} dt e^{i\omega t}\langle \hat{b}^\dagger_{\mathrm{out},R}(0)\hat{b}_{\mathrm{out},R}(t)\rangle \quad (25)$$

Note that this corresponds to the power that would be measured by a photomultiplier; we will first analyze this spectrum, and then turn to the case relevant here, the spectrum measured by a voltage amplifier.

We will be interested in the form of the Lorentzian resonance corresponding to the mechanical motion that will appear in $S_R[\omega]$ near the cavity resonance frequency. Returning to the lab frame (i.e. not in the rotating frame used to derive the equations), one finds for $|\delta| \ll \kappa \ll \omega_m$ from Eq. (24):

$$S_R[\delta] = \frac{4\kappa_R \Gamma_m^T}{\kappa^2} \frac{\alpha^2}{\delta^2 + \Gamma_{\rm tot}^2/4} \cdot \bar{n}_m^T + \frac{4\kappa_R}{\kappa} \sum_{j=L,I} \frac{\kappa_I}{\kappa} \left| 1 - \frac{2\alpha^2/\kappa}{-i\delta + \Gamma_{\rm tot}/2} \right|^2 \cdot \bar{n}_j^T \tag{26}$$

Here, $\Gamma_{\rm tot} = \Gamma_m^T + \Gamma_{\rm opt}$ is the total mechanical damping. The first term in Eq. (26) corresponds to the contribution from the intrinsic thermal noise driving the mechanics, while the second term corresponds to the contribution from the thermal noise driving the cavity. We see that there is interference between the direct influence of this noise on the cavity, and the back-action effect of this noise. Specializing now to the good cavity limit $\omega_m \gg \kappa$ relevant to the experiment, some algebra now yields:

$$S_R[\delta] = \frac{4\kappa_R}{\kappa} \cdot \bar{n}_{sr}^T + \frac{\kappa_R}{\kappa_{\rm tot}} \Gamma_{\rm opt} \frac{\Gamma_{\rm tot}}{\delta^2 + \Gamma_{\rm tot}^2/4} \cdot \bar{n}_{\rm eff} \tag{27}$$

where the weight of the Lorentzian oscillator resonance is controlled by the the parameter

$$\bar{n}_{\rm eff} = \bar{n}_m - 2\bar{n}_{sr}^T \tag{28}$$

Thus, the oscillator's motion manifests itself as a Lorentzian centered at the cavity resonance frequency. Because of the interference effects described above, this Lorentzian can either be a peak or a dip. By measuring the weight of this Lorentzian, one can extract the parameter $\bar{n}_m$, and hence the average number of quanta in the mechanical resonator. We stress that the interference effects here only play a role in determining the form of the output spectrum, but do not alter the state of the mechanical resonator. The mechanical resonator will be in a thermal state with an average number of quanta given by $\bar{n}_m$.

Note that the above results pertain to the output spectrum measured by a photomultiplier. In microwave experiments, the output spectrum is instead measured using a voltage amplifier. As a result, one measures the symmetric-in-frequency noise spectrum $\bar{S}_R[\omega]$ given by:

$$\bar{S}_R[\omega] \equiv \frac{1}{2} \int_{-\infty}^{\infty} dt e^{i\omega t} \langle \{ \hat{b}_{{\rm out},R}(t), \hat{b}_{{\rm out},R}^\dagger(0) \} \rangle \tag{29}$$

Unlike $S_R[\omega]$, the above spectrum will be sensitive to zero-point fluctuations. One can easily show however that near the cavity resonance, the form of the oscillator resonance in $\bar{S}_R[\omega]$ is identical to what was found above:

$$\bar{S}_R[\delta] = 1 + \frac{4\kappa_R}{\kappa} \cdot \bar{n}_{sr}^T + \frac{\kappa_R}{\kappa_{\rm tot}} \Gamma_{\rm opt} \frac{\Gamma_{\rm tot}}{\delta^2 + \Gamma_{\rm tot}^2/4} \cdot \bar{n}_{\rm eff} \quad (30)$$

The only difference between the two spectra in the relevant $\omega_m \gg \kappa$ limit is in the form of the noise floor. The weight of the Lorentzian oscillator resonance / anti-resonance is the same in both cases, and hence the method for extracting $\bar{n}_m$ from $\bar{n}_{\rm eff}$ is the same as discussed above.

Finally, to extract the parameter $\bar{n}_{sr}^T$, one needs to look at the weight of the entire cavity resonance in the output spectrum. Focusing now on this resonance, and ignoring the small contribution from the oscillator near $\omega = \omega_{sr}$, we have:

$$\bar{S}_R[\omega] = 1 + \frac{\kappa_R}{\kappa} \frac{\kappa^2}{(\omega - \omega_{sr})^2 + (\kappa/2)^2} \bar{n}_{sr}^T \quad (31)$$

Thus, by considering the weight of the entire cavity resonance in the output spectrum, one can obtain $\bar{n}_{sr}^T$.

References

[1] L. Frunzio, A. Wallraff, D. Schuster, J. Majer, and R. Schoelkopf. Fabrication and characterization of superconducting circuit qed devices for quantum computation. *IEEE Trans Appl Supercon*, 15 (2):860–863, 2005.

[2] David Pozar. *Microwave Engineering*. John Wiley, 2005.

[3] J.B. Hertzberg. *Back-Action Evading Measurements of Nanomechanical Motion Approaching Quantum Limits*. PhD thesis, University of Maryland, College Park, 2009.

[4] Florian Marquardt, Joe P. Chen, A. A. Clerk, and S. M. Girvin. Quantum theory of cavity-assisted sideband cooling of mechanical motion. *Phys. Rev. Lett.*, 99:093902, 2007.

[5] J.D. Teufel, J.W. Harlow, C. A. Regal, and K.W. Lehnert. Dynamical backaction of microwave elds on a nanomechanical oscillator. *Phys. Rev. Lett.*, 101:197203, 2008.

[6] V. B. Braginsky and S. P. Vyatchanin. *Phys. Lett. A*, 293(228), 2002.

[7] F. Marquardt, J. P. Chen, A. A. Clerk, and S. M. Girvin. Quantum theory of cavity-assisted sideband cooling of mechanical motion. *Phys. Rev. Lett.*, 99:093902, 2007.

[8] I. Wilson-Rae, N. Nooshi, W. Zwerger, and T. J. Kippenberg. Theory of ground state cooling of a mechanical oscillator using dynamical backaction. *Phys. Rev. Lett.*, 99:093901, 2007.

[9] Florian Marquardt, A A Clerk, and S M Girvin. Quantum theory of optomechanical cooling. *J. Mod. Opt.*, 55:19, 2008.

[10] J. M. Dobrindt, I. Wilson-Rae, and T. J. Kippenberg. Parametric normal-mode splitting in cavity optomechanics. *Phys. Rev. Lett.*, 101:263602, 2008.

[11] D. F. Walls and G. J. Milburn. *Quantum Optics*. Springer, Berlin, 1994.

[12] A. A. Clerk, M. H. Devoret, F. Marquardt, S M Girvin, and R. J. Schoelkopf. Introduction to quantum noise, measurement and amplification. *arXiv:08104729*, 2008.